Water Supersaturation for Early Mars

A. Delavois, F. Forget, M. Turbet, E. Millour, R. Vandemeulebrouck, L. Lange, A. Bierjon

Water Supersaturation for Early Mars

A.Delavois[1], F.Forget[1], M.Turbet[1], E.Millour[1], R.Vandemeulebrouck[1], L.Lange[1], A.Bierjon[1]

[1]Laboratoire de Météorologie Dynamique/IPSL, Sorbonne Université, ENS, PSL Research University,Ecole Polytechnique, CNRS, Paris France

Key Points:

- We simulated water supersaturation in an Early Mars climate considering an abundant source of water on the surface and an arid scenarios;
- Supersaturation can warm Early Mars only with unrealistic supersaturation ratios;
- Supersaturation is only efficient when it occurs in the lower layers of the atmosphere in our simulations.

Corresponding author: Antony Delavois, `antony.delavois@lmd.ipsl.fr`

Abstract

Evidence of past liquid water flowing on the surface of Mars has been identified since the first orbital mission to the planet. However, reconstructing the climate that would allow liquid water at the surface is still a intense area of research. Previous studies showed that an atmosphere composed only of CO_2 and H_2O could not sustain surface temperatures above the freezing point of water. Different solutions have been studied, ranging from events like impacts to different atmospheric compositions, or even a radiative feedback of water clouds that would create a dramatic greenhouse effect. In this context, we propose to study if the supersaturation of water could warm the planet. Strong supersaturation is observed in the present-day martian atmosphere. On early Mars supersaturation could enhance the greenhouse effect through the strong absorption of the IR flux of water vapor or by modifying water clouds. While 1D modeling suggest a significant impact, our 3D model show that warming the climate of Early Mars require high supersaturation ratio, especially in the lower layers of the atmosphere. This configuration seems highly unrealistic, since the level of supersaturation are higher than what would be expected in a dense atmosphere.

1 Introduction

Rovers and orbiters sent to Mars have provided us with compelling evidence for abundant liquid water flowing on the surface in the early days of the planet, during the Noachian and Hesperian eras. One of the biggest challenge in planetary science is to reconcile these geological and mineralogical features with a corresponding climate despite a fainter Sun irradiating approximately less than a third of today's Earth received energy (Gough, 1981; Sagan & Mullen, 1972). Some recent studies found that a reduced thick atmosphere, mainly composed of CO_2, H_2O and H_2, could sustain a warm climate for periods long enough and explain the presence of valley networks (Ramirez et al., 2014; Wordsworth, 2016; Turbet & Forget, 2022). However, explaining the entire Noachian / Hesperian era with this only scenario is unlikely since dramatic climate changes must have occured during this 1 Gy long period. For instance, it is difficult to reconcile the presence of Mn-rich rocks, that could only be created within a wet and oxidized environment, with a consequent amount of H_2 in the atmosphere (Lanza et al., 2016). This is one reason in order to keep searching for new processes or events that can be responsible of a substantial greenhouse effect.

A recent study suggests that H_2O_2 could have provided a sufficient greenhouse effect, assuming that H_2O_2 supersaturation occurs in the upper layers of the atmosphere (Ito et al., 2020). Given that water can be much more abundant and can absorb in the same window than H_2O_2, what about water supersaturation?

Moreover, supersaturation could have an effect on clouds by raising the hygropause. It would create higher and cooler clouds with a subsequently stronger greenhouse effect, leading to a potential warming of the surface. The cirrus clouds greenhouse warming hypothesis has been previously studied, first in the context of a post-impact climate (Segura et al., 2002, 2008, 2012) that showed promising results to sustain a warm climate over a relatively long period, although this was shown to be overestimated by (Turbet et al., 2017) because of convection and condensation processes. Other studies suggest that clouds could provide a warming but only under very specific assumptions on microphysics or ice location (Urata & Toon, 2013; Ramirez & Kasting, 2017; Kite et al., 2021) .

On current-day Mars, water in excess to saturation has been observed in the atmosphere (Maltagliati et al., 2011; Fedorova et al., 2018, 2020), and is sometimes associated with the formation of water clouds. Supersaturation ratio are able to reach as much as 10 around 30-40 km (Maltagliati et al., 2011) and even up to 300 in the upper atmosphere of Mars, around 80km (Fedorova et al., 2020). It has been noticed that supersaturation in the top part of cirrus clouds is enhanced during the dusty season and in particular during Global Dust Storms, reaching ratio of 5 at approximately 60-70 km (Poncin et al., 2022).

This phenomenon is also observed on Earth in the upper troposphere, and is mostly associated with the formation of cirrus clouds (Heymsfield et al., 2017; Krämer et al., 2020). It has also been observed near the surface on the icy desert of Antarctica (Genthon et al., 2017). Supersaturation ratios in cirrus clouds are limited by the formation of ice particles from either homogeneous or heterogeneous nucleation (Vali et al., 2015; Baumgartner et al., 2022). Relative humidity in these conditions is not exceeding 200% (Krämer et al., 2009; Lamquin et al., 2012), which is also the order of magnitude observed in Antarctica (Genthon et al., 2017). Some water ice particles are sometimes found in the summertime high-latitude mesosphere, creating supersaturation ratio exceeding 10^5 and then giving birth to noctilucent clouds (Murray & Jensen, 2010). This ratio is constrained by the homogeneous nucleation from the vapor phase and thus can be considered as an extreme upper limit for our study. However, reaching these levels of saturation in the lower atmosphere seems unrealistic.

In this paper, using 1D and 3D climate models, we try to establish the potential of water supersaturation for warming the surface of Early Mars. We do not consider any a priori assumption concerning supersaturation limitation or origin, excepted that the source of water is located at the surface of the planet for 3D simulations. We tested two set of simulations in order to explore the sensitivity to available water, with a relatively arid simulation and an idealistic extremely wet simulation.

2 Methods

2.1 General Description

For this study, we used the LMD Generic Global Climate Model both in its 1D and 3D versions, adapted to typical Noachian conditions. The Early Mars climates have already been studied with this model including full CO_2 and water cycles (Forget et al., 2013; Wordsworth et al., 2013; Turbet et al., 2017; Turbet & Forget, 2019, 2022). and a full description of the model can be found in Forget et al. (2013) and Wordsworth et al. (2013). We assume a mean surface pressure of 2 bar because it is the optimum pressure for warming an atmosphere mainly composed of CO_2 (Forget et al., 2013, Fig. 1). The solar flux is 75 % of today's, giving a mean solar flux on Mars of 111 W/m².

This paper first presents global averaged 1D simulations vertically divided into 34 layers (up to $\sim$1 Pa or 100 km). Water is only considered as a radiatively active gas in the atmospheric composition. We do not consider a full water cycle, since evaporation, condensation and rain are neglected in the 1D simulations. The effects of water clouds are not included in the 1D simulations but we explore the role of water clouds by implementing a full water cycle in 3D simulations. However, CO_2 clouds are taken into account and CO_2 microphysics is performed with a Cloud Condensation Nuclei (CCN) density of 1000 particles/kg. We tuned this parameter in order to model a global greenhouse effect analogous to the one obtained in 3D by Wordsworth et al. (2013).

3D simulations were performed with a horizontal resolution of 32$\times$32 in longitude $\times$ latitude. The vertical dimensions is split into 15 layers with altitudes up to $\sim$1000 Pa. Vertical layers are described using hybrid coordinates.

We used the pre-True Polar Wander (pre-TPW) topography from Bouley et al. (2016) that demonstrated the formation of late Noachian valley networks is likely to have predated the formation of most of the Tharsis volcanic buldge. The pre-TPW topography is based on present-day MOLA topography but without Tharsis and all the younger volcanic features. It also takes into account that a True Polar Wander event of 20°-25° occured during the rise of Tharsis.

Because the water content during Noachian is poorly constrained, we explore two different scenarios for available water in the climate system. First, we use a relatively dry initial state where ice is mainly located on cold traps, i.e. high altitude areas and poles. This initial state comes from the simulation presented in Bouley et al. (2016, Fig. 2b) and is therefore considered as realistic, although it has been done for a mean surface pressure of 0.2 bar. Global equivalent layer of ice is approximately 37 mm thick.

The other set of 3D simulations is performed with an idealistic wet set-up designed to overestimate the amount of water vapor in the atmosphere and thus the greenhouse effect. We initialize simulations with a global ice sheet of 10m covering the entire planet. In order to maximise water in the atmosphere, we set the albedo of the ice to 0.2, which is usually the albedo of bare ground. Combined to an obliquity of 40°, these simulations are designed to explore the supersaturation scenario for an idealistic extremely wet case.

2.2 Modeling Supersaturation

2.2.1 Supersaturation in the 1D model

Supersaturation is implemented in a simple way for 1D simulations. At the end of each time step, we calculate the water mass mixing ratio (mmr) at saturation in each layer using the Clausius-Clapeyron equation. Then this mass mixing ratio of water is multiplied by a supersaturation ratio ($sursat$ parameter). A pressure limit of supersaturation ($plim$) is added to the model in order to allow supersaturation only above a certain level. If the pressure of a given layer is higher than $plim$, the supersaturation ratio is set equal to 1 (saturation). In these 1D simulations, the water mixing ratio is not free to evolve and is at least the mixing ratio at saturation.

2.2.2 Supersaturation in the 3D model

In order to allow supersaturation, the model has been modified where condensation and cloud formation are involved. The cloud formation is mainly described by a large-scale condensation scheme, a moist convective adjustment (Manabe & Wetherald, 1967), and vertical mixing of the boundary layer (Wordsworth et al., 2013; Turbet et al., 2017). In the large scale condensation scheme, condensation occurs when the water mass mixing ratio is above a relative humidity $RH = 100\%$ or $RH = sursat(\geq\ 100\%)$ depending on the pressure of the layer and the $plim$ parameter, similarly to the description of the 1D model.

3 Results

3.1 1D model

Figure 1 shows the evolution of the surface temperature of our 1D model with the supersaturation parameter $sursat$. Two sets of simulations are shown. The blue line represented with dots shows results obtained with radiatively active CO_2 clouds, the crossed orange line being with inactive radiative clouds. It can be inferred that there is no major feedback of supersaturation on the greenhouse effect of CO_2 clouds with the chosen microphysics parameters, the difference between the two curves being almost constant. Surface temperature reaches the freezing point of water for supersaturation ratio around 10. Since the surface pressure is 2 bar, it requires lower layers to be supersaturated at levels much higher than what is observed today in cirrus clouds which can be seen as unrealistic. We can observe supersaturation levels greater than 10 in today's Mars but the pressure is much more lower in these layers of the atmosphere (Maltagliati et al., 2011).

Figure 2 illustrates the need of supersaturation occurring in the lower layers in order to have a significant greenhouse effect. The effect of supersaturation is limited to a few Kelvins if it is only above 1 bar (∼8 km) and there is no effect if it occurs only above 0.5 bar (∼17 km).

We can observe significant warming with $plim < 0.5\ bar$ only for high supersaturation ratio (not shown). For example, simulations reach a surface temperature of 282 K (275 K) for a $sursat$ ratio of 10^5 and a $plim$ parameter of 0.2 bar (0.1 bar) respectively. This scenario would imply a high production of H_2O in the upper layers of the atmosphere and not only a transport of water from the surface to higher layers.

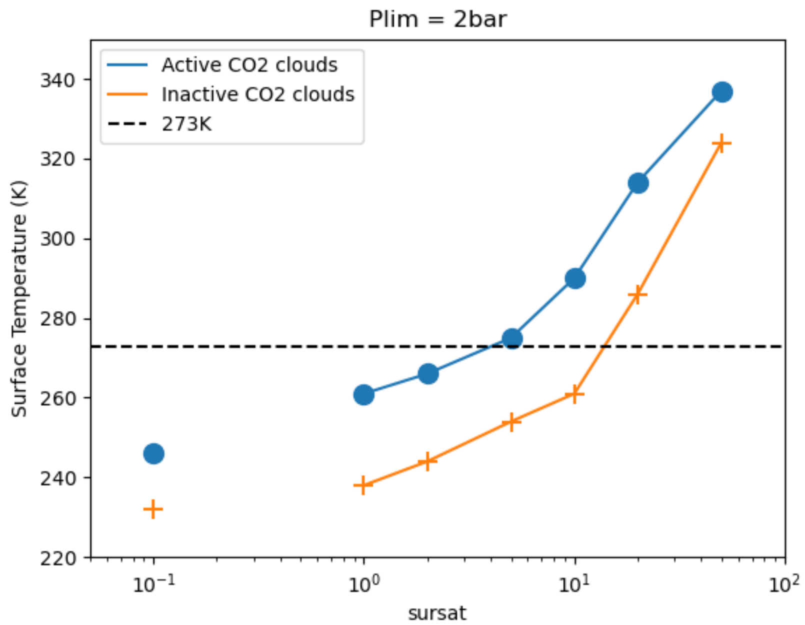

Figure 1. Surface Temperature as a function of supersaturation ratio for 1D simulation. Supersaturation is allowed down to the surface (*plim*=ps). Surface pressure is 2 bar.

3.2 Effect of supersaturation in 3D models

The 1D results suggest that water supersaturation could warm Early Mars, assuming that it would occur everywhere and especially in the lower atmosphere. To further investigate if this is possible, and to explore the feedback between clouds and supersaturation, a 3D model is needed.

3.2.1 Arid Simulation

The first set of simulations is performed with mean surface pressure of 2 bar and relatively dry initial conditions as described in section 2.1. Water ice is mainly located on the high region near the current location of Tharsis (Bouley et al., 2016, Fig. 2) and the global water content is 33mm GEL mainly of ice on the surface (10pr-µm of water ice clouds, 390pr-µm of water vapor). A reference simulation is performed without supersaturation. The average mean temperature is 253K consistent with Wordsworth et al. (2013). Figure 3 shows the mean annual surface temperature for different simulations performed from this dry initial state. In Figures 4 and 5, the relative humidity RH and

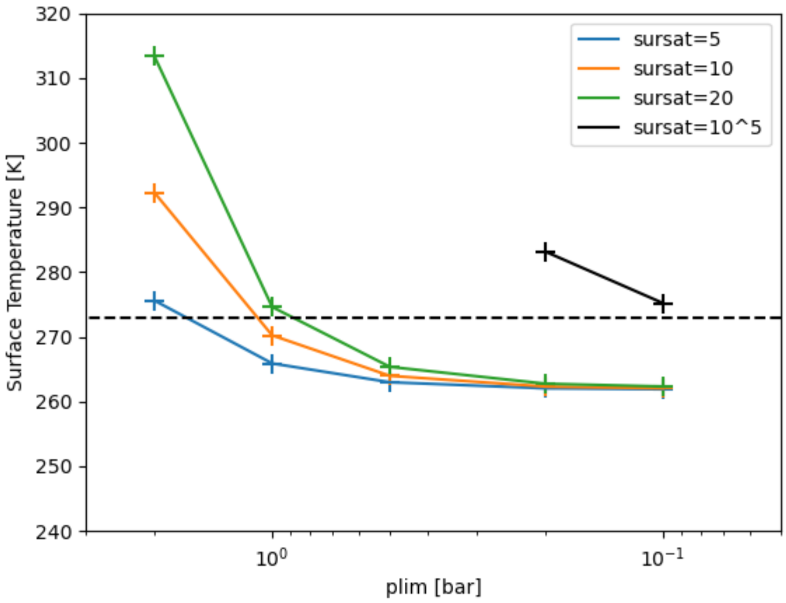

Figure 2. Surface Temperature as a function of pressure limit of supersaturation for 1D simulation and for different supersaturation ratio. Surface pressure is 2 bar.

cloud density are respectively shown, for the same simulations. Global mean temperature and planetary albedo are indicated for these simulations.

As expected for such surface pressure (Forget et al., 2013, Fig. 7), local surface temperatures are influenced by adiabatic warming and cooling mechanisms and we can see that the northern plains are globally warmer (around 20K) than the southern hemisphere for all simulations, except for Hellas basin. As expected from the 1D study (Figure 2), supersaturation is only efficient when it occurs in the lower layers of the atmosphere. Here, for a *sursat* parameter of 10 (3b, c, d), there is no warming when supersaturation is assumed only above the 0.5 bar level. Figure 3e confirms that even with high supersaturation ratio, there is no significant warming if the *plim* parameter is less than 0.5 bar. Simulation with even higher *sursat* ratio (not shown in this paper) does not present significantly rising temperature since water vapor struggles to reach the higher layers of the atmosphere.

Annual and zonal mean relative humidity profiles are shown in Figure 4. The reference simulation (Figure 3a) depicts a maximum zone of relative humidity between 0.5 and 1 bar. This optimum zone corresponds to a hygropause (see Figure 5) and the higher layers above 0.1 bar are relatively dry. A similar pattern is observed for simulations where supersaturation is uniformly allowed down to the surface (Figure 3b and f). If supersaturation is allowed only from 1 bar (Figure 3d), the wet area is thinner and it even vanishes when supersaturation is allowed only from 0.5 bar (Figure 3c and e). As a consequence, our simulations can not fully supersaturate the layers above 0.5 bar and are unable to create a significant warming even with high supersaturation ratio.

Zonally and annually averaged cloud density is shown in Figure 5. In the reference simulation (Figure 5a), clouds are mainly located around the pressure level of 1 bar and vertically limited by a hygropause at approximately 0.5 bar. The pattern is identical for simulations with $sursat \leq 1\ bar$ (Figure 5c,d,e) and we observe a slight shift towards

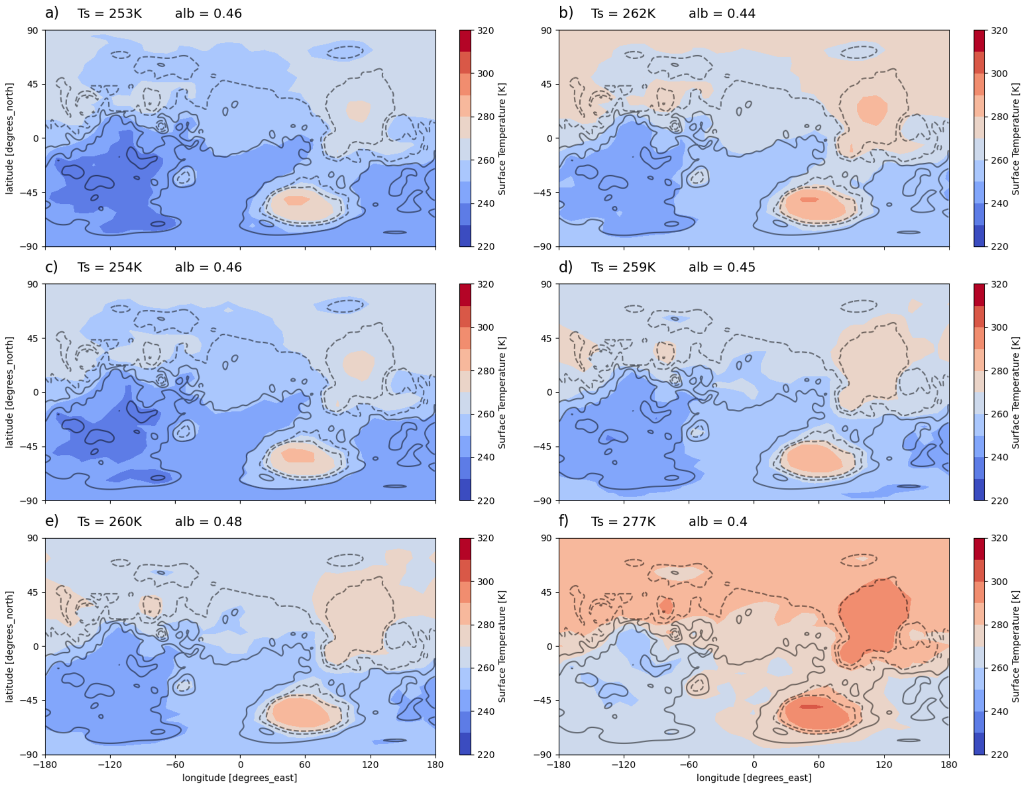

Figure 3. Annual mean surface temperature for an arid scenario with a mean surface pressure of 2 bar. *sursat* and *plim* are the two parameters of the supersaturation model, respectively for the maximal supersaturation ratio allowed and the maximal pressure where supersaturation can occur. a) Reference simulation, *sursat*=1; b) *sursat*=10, *plim*=ps; c) *sursat*=10 *plim*=0.5 bar; d) *sursat*=10 *plim* 1 bar; e) *sursat*=1000 *plim*=0.5 bar; f) *sursat*=100 *plim*=ps. Global mean surface temperature and Bond albedo are indicated.

higher altitudes when $plim = p_s$ (Figure 5b). For the extreme case simulation with $sursat$=100 (Figure 5f), water clouds are totally removed from the atmosphere. A simulation similar to the reference simulation but performed without the radiative effect of clouds (not shown here) shows that clouds have a limited impact on the global surface temperature. Thus, in the case of arid simulations, the warming observed with high *sursat* values is fully related to the quantity of water vapor in the atmosphere, which absorbs the emitted IR flux.

3.2.2 Idealized Wet Simulation

This scenario is designed in order to maximize the amount of water vapor in the atmosphere, assuming that there is no significant photochemical source in the atmosphere. Although if this is not physically realistic, because we set a unusually low albedo for the ice (0.2, typical of bare soil) this scenario allows to explore if the atmospheric circulation limit the amount of water vapor when surface sources are abundant. Similarly to the arid scenario, Figures 6, 7, 8 respectively describe annual mean surface temperature, zonal and annual average of relative humidity and cloud density. Even with a water content significantly higher in this idealized wet scenario (see Table 1), the simulations are not able to reach a global mean surface temperature above the freezing point

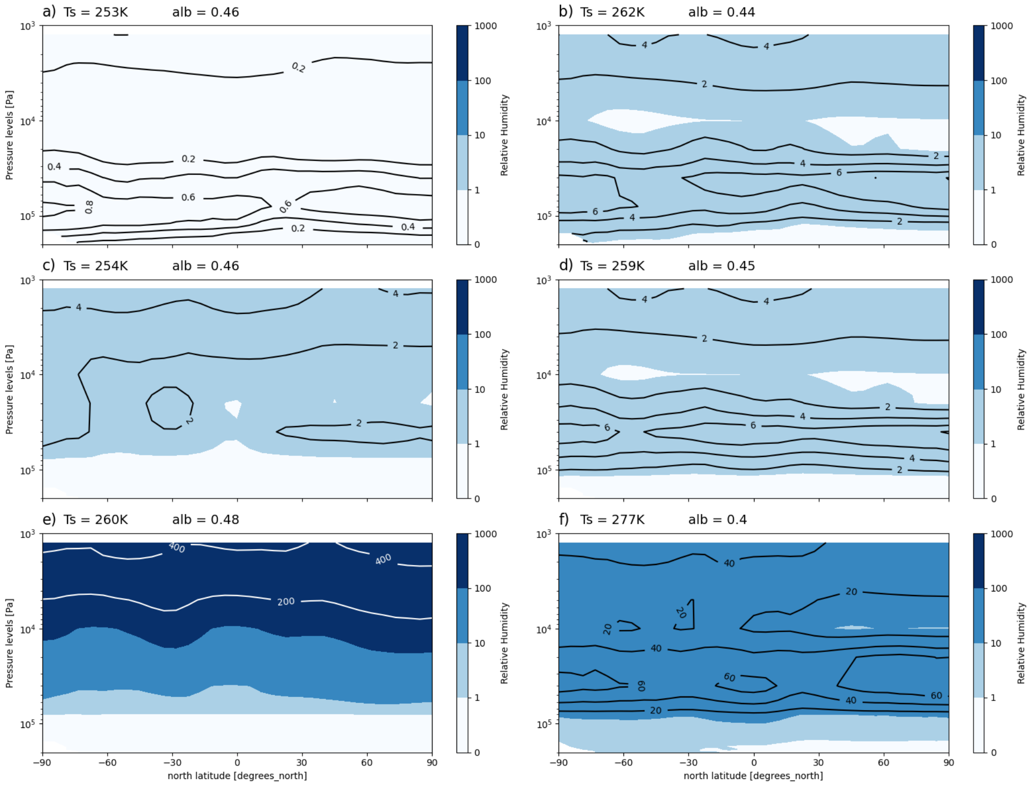

Figure 4. Annual and zonal mean relative humidity for an arid scenario with a mean surface pressure of 2 bar. *sursat* and *plim* are the two parameters of the supersaturation model, respectively for the maximal supersaturation ratio allowed and the maximal pressure where supersaturation can occur. a) Reference simulation, *sursat*=1; b) *sursat*=10, *plim*=ps; c) *sursat*=10 *plim*=0.5 bar; d) *sursat*=10 *plim* 1 bar; e) *sursat*=1000 *plim*=0.5 bar; f) *sursat*=100 *plim*=ps. Global mean surface temperature and Bond albedo are indicated.

of water, excepted for the *sursat*=100 simulation, that is described further. Surface temperatures are even slightly colder than in the arid scenario.

Surface temperatures are lower mainly because of the high albedo of clouds that cover a large part of the planet. This negative feedback is not compensated by a strong enough greenhouse effect. As shown in Figure 8. The high amount of water injected in the atmosphere from the initial ice sheet create thick low clouds (Figure 8a,c,d,e) with a net cooling effect. Supersaturation is able to raise the forming altitude of clouds and reduce the total planetary albedo (Figure 8b,f) but only when supersaturation is allowed from the ground to the top of the atmosphere.

Similarly to the arid scenario, we observe that water vapor is not fully supersaturated in the highest levels of the atmosphere, especially for simulations with low *sursat* or *plim* parameters (Figure 7). The simulation with a high *sursat* ratio (Figure 7e) reaches slightly lower relative humidity in the upper layers compared to the arid simulation and still is not able to provide a significant warming, despite our ambition to model a more humid atmosphere in this scenario. As a consequence, we are not able to create a highly supersaturated layer in the upper atmosphere as it is done in Ito et al. (2020) with H_2O_2.

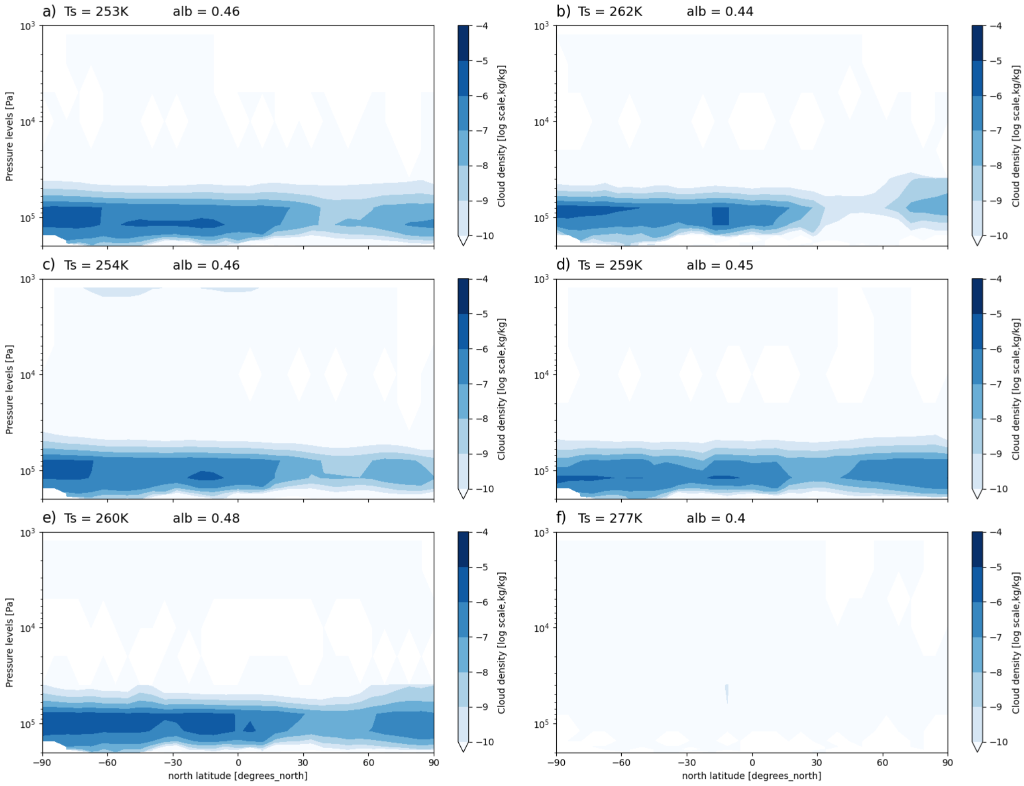

Figure 5. Annual and zonal mean water ice cloud density (kg/kg, log scale) for an arid scenario with a mean surface pressure of 2 bar. *sursat* and *plim* are the two parameters of the supersaturation model, respectively for the maximal supersaturation ratio allowed and the maximal pressure where supersaturation can occur. a) Reference simulation, *sursat*=1; b) *sursat*=10, *plim*=ps; c) *sursat*=10 *plim*=0.5 bar; d) *sursat*=10 *plim* 1 bar; e) *sursat*=1000 *plim*=0.5 bar; f) *sursat*=100 *plim*=ps. Mean surface temperature and Bond albedo are indicated.

The extreme case presented in Figure 7f is surprising in the fact that the surface temperature pattern is not similar to others simulations. In fact, due to the high quantities of water in the layers where the pressure is above 2 bar, we observe a decrease of the incident solar flux at the surface due to the absorption of the water vapor in the solar spectrum range. This creates a pattern where low-altitude regions such as the Hellas bassin or Elysium Planitia have lower surface temperature than areas located at higher altitude. The effect of a high *sursat* ratio is interesting regarding clouds, because it raise the altitude of clouds which are also less dense. The global result is a lower cooling effect of clouds, since high cirrus clouds are expected to create a stronger greenhouse effect (Ramirez & Kasting, 2017). This simulation shows a global mean surface temperature above the freezing point of water and more interestingly in the southern areas, where valley networks are currently observed. However, the supersaturation levels and the quantity of water in the atmosphere is totally unrealistic.

4 Conclusions

Using 1D and 3D global climate models, We investigated the potential impact of a water supersaturation for warming a CO_2-dominated atmosphere on Early Mars. Our 1D results showed that supersaturation could warm the planet considering high super-

Table 1. Yearly Global Water Content (kg/m^2)

Simulation	Surface Ice	Clouds particles	Vapor
DRY Ref	32.6	0.010	0.4
DRY S10	28.8	0.007	4.0
IC Ref	9938	0.10	1.6
IC S10	9986	0.06	16.3

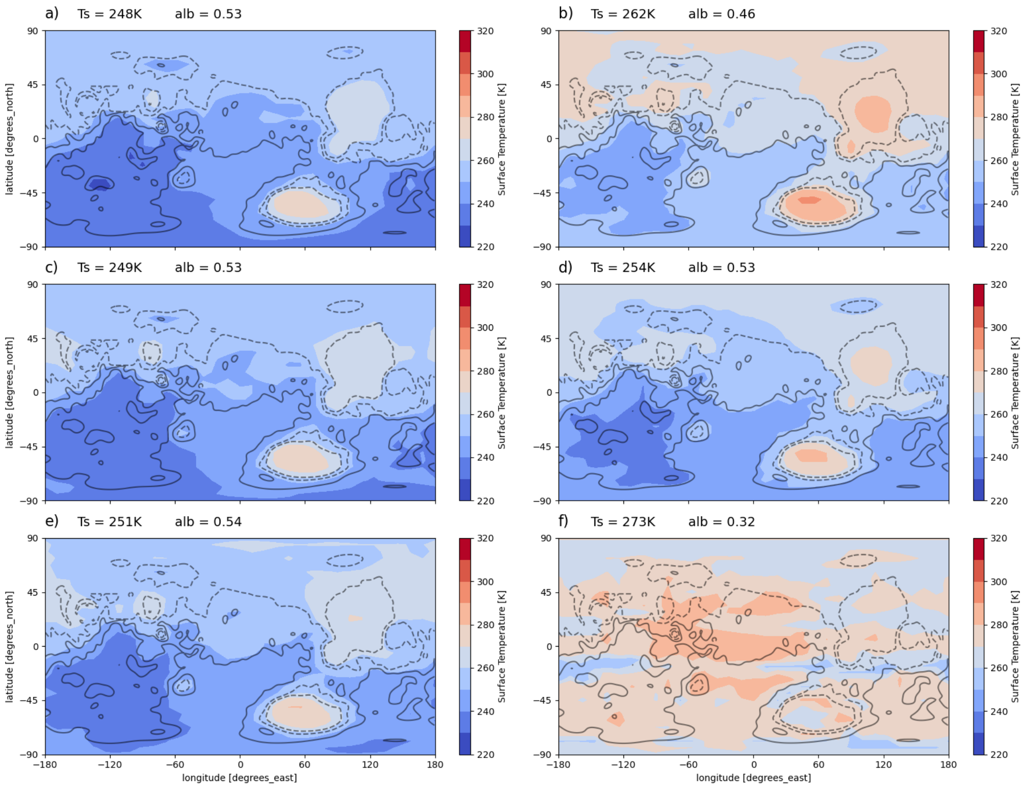

Figure 6. Annual mean surface temperature for an idealized wet scenario with a mean surface pressure of 2 bar. *sursat* and *plim* are the two parameters of the supersaturation model, respectively for the maximal supersaturation ratio allowed and the maximal pressure where supersaturation can occur. a) Reference simulation, *sursat*=1; b) *sursat*=10, *plim*=ps; c) *sursat*=10 *plim*=0.5 bar; d) *sursat*=10 *plim* 1 bar; e) *sursat*=1000 *plim*=0.5 bar; f) *sursat*=100 *plim*=ps. Global mean surface temperature and Bond albedo are indicated.

saturation ratio in every layer of the atmosphere, especially the lower layers. This conclusion is tempered by 3D results, where we reached a relevant warming with supersaturation ratio highly unrealistic in the lower layers of a dense atmosphere.

Additionally, we demonstrated that supersaturation can create higher altitude clouds both in our arid and idealized wet simulation with water sources on the surface. This raise of water clouds is however seen only with supersaturation occurring from the ground and is not enough to create a sustainable warming of the surface in most of our simulations. An extreme case with unrealistic supersaturation ratio of 100 creates a signif-

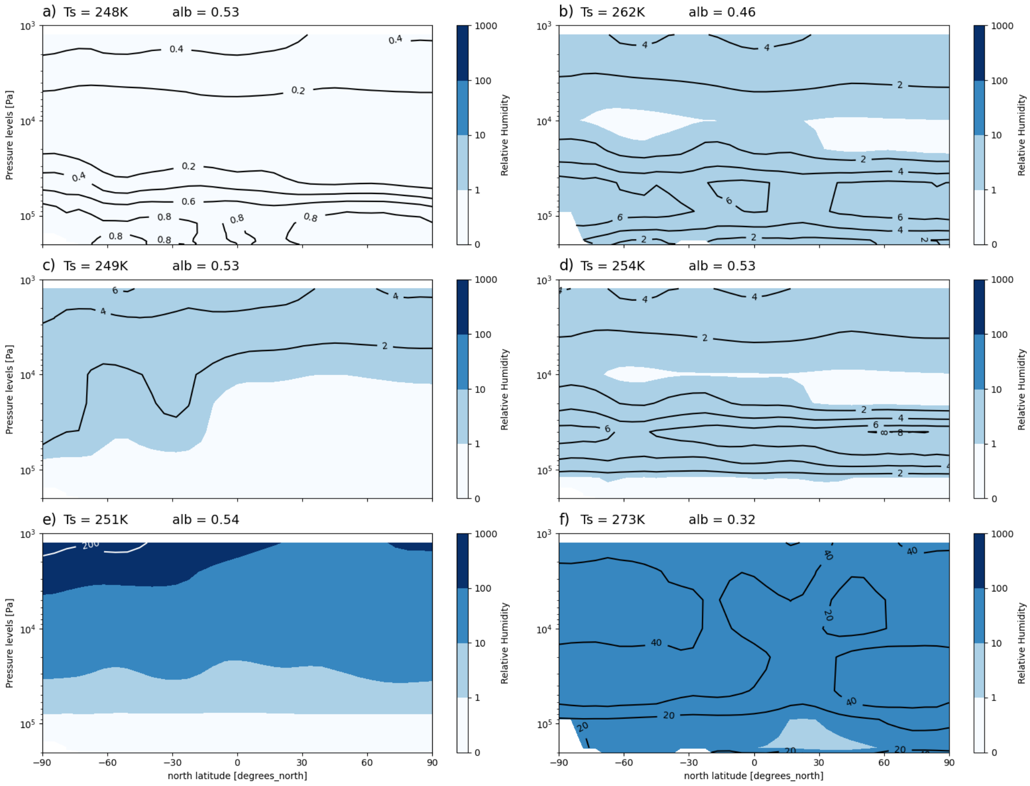

Figure 7. Annual and zonal mean relative humidity for an idealized wet scenario with a mean surface pressure of 2 bar. *sursat* and *plim* are the two parameters of the supersaturation model, respectively for the maximal supersaturation ratio allowed and the maximal pressure where supersaturation can occur. a) Reference simulation, *sursat*=1; b) *sursat*=10, *plim*=ps; c) *sursat*=10 *plim*=0.5 bar; d) *sursat*=10 *plim* 1 bar; e) *sursat*=1000 *plim*=0.5 bar; f) *sursat*=100 *plim*=ps. Global mean surface temperature and Bond albedo are indicated.

icant warming, associated to a high amount of water vapor in the atmosphere and a higher cloud layer.

5 Open Research

Data files for figures used in this analysis are available in a public repository, see Delavois et al. (2022).

Acknowledgments

This project has received funding from the European Research Council (ERC) under the European Union's Horizon 2020 research and innovation programme (grant agreement No 835275).

The authors acknowledge the exceptional computing support from Grand Equipement National de Calcul Intensif (GENCI) and Centre Informatique National de l'Enseignement Supérieur (CINES). All the simulations presented here were carried out on the Occigen cluster hosted at CINES.

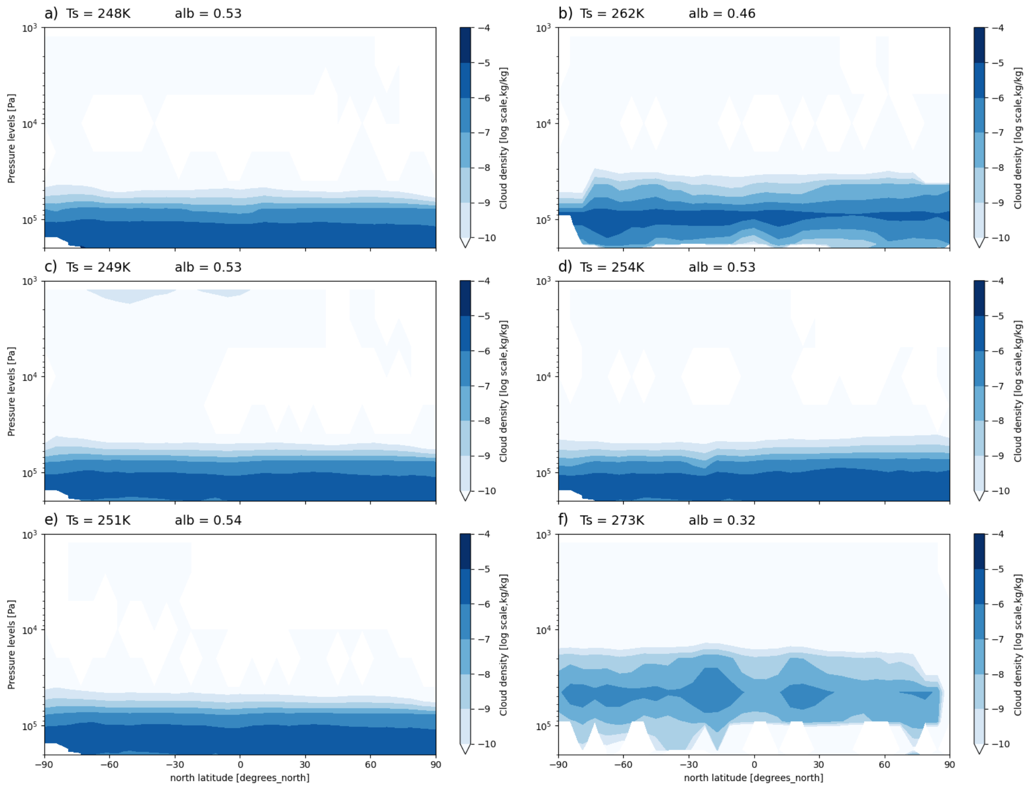

Figure 8. Annual and zonal mean water ice cloud density (kg/kg, log scale) for an idealized wet scenario with a mean surface pressure of 2 bar. *sursat* and *plim* are the two parameters of the supersaturation model, respectively for the maximal supersaturation ratio allowed and the maximal pressure where supersaturation can occur. a) Reference simulation, *sursat*=1; b) *sursat*=10, *plim*=ps; c) *sursat*=10 *plim*=0.5 bar; d) *sursat*=10 *plim* 1 bar; e) *sursat*=1000 *plim*=0.5 bar; f) *sursat*=100 *plim*=ps. Mean surface temperature and Bond albedo are indicated.

References

Baumgartner, M., Rolf, C., Grooß, J.-U., Schneider, J., Schorr, T., Möhler, O., ... Krämer, M. (2022, January). New investigations on homogeneous ice nucleation: the effects of water activity and water saturation formulations. *Atmospheric Chemistry & Physics*, *22*, 65–91. Retrieved 2022-02-21, from `https://ui.adsabs.harvard.edu/abs/2022ACP....22...65B` (ADS Bibcode: 2022ACP....22...65B) doi: 10.5194/acp-22-65-2022

Bouley, S., Baratoux, D., Matsuyama, I., Forget, F., Séjourné, A., Turbet, M., & Costard, F. (2016, March). Late Tharsis formation and implications for early Mars. *Nature*, *531*, 344–347. Retrieved 2021-12-09, from `https://ui.adsabs.harvard.edu/abs/2016Natur.531..344B` (ADS Bibcode: 2016Natur.531..344B) doi: 10.1038/nature17171

Delavois, A., F.Forget, M.Turbet, E.Millour, R.Vandemeulebrouck, L.Lange, & A.Bierjon. (2022). *Water Supersaturation for Early Mars.* Harvard Dataverse. Retrieved from `https://doi.org/10.7910/DVN/O94VWV` doi: 10.7910/DVN/O94VWV

Fedorova, A., Bertaux, J.-L., Betsis, D., Montmessin, F., Korablev, O., Maltagliati, L., & Clarke, J. (2018, January). Water vapor in the middle atmosphere of

Mars during the 2007 global dust storm. *Icarus*, *300*, 440–457. Retrieved 2022-02-21, from https://ui.adsabs.harvard.edu/abs/2018Icar..300..440F (ADS Bibcode: 2018Icar..300..440F) doi: 10.1016/j.icarus.2017.09.025

Fedorova, A., Montmessin, F., Korablev, O., Luginin, M., Trokhimovskiy, A., Belyaev, D. A., ... Wilson, C. F. (2020, January). Stormy water on Mars: The distribution and saturation of atmospheric water during the dusty season. *Science*, *367*, 297–300. Retrieved 2021-08-04, from https://ui.adsabs.harvard.edu/abs/2020Sci...367..297F doi: 10.1126/science.aay9522

Forget, F., Wordsworth, R., Millour, E., Madeleine, J. B., Kerber, L., Leconte, J., ... Haberle, R. M. (2013, January). 3D modelling of the early martian climate under a denser CO2 atmosphere: Temperatures and CO2 ice clouds. *Icarus*, *222*, 81–99. Retrieved 2021-08-13, from https://ui.adsabs.harvard.edu/abs/2013Icar..222...81F (ADS Bibcode: 2013Icar..222...81F) doi: 10.1016/j.icarus.2012.10.019

Genthon, C., Piard, L., Vignon, E., Madeleine, J.-B., Casado, M., & Gallée, H. (2017, January). Atmospheric moisture supersaturation in the near-surface atmosphere at Dome C, Antarctic Plateau. *Atmospheric Chemistry & Physics*, *17*, 691–704. Retrieved 2022-02-21, from https://ui.adsabs.harvard.edu/abs/2017ACP....17..691G (ADS Bibcode: 2017ACP....17..691G) doi: 10.5194/acp-17-691-2017

Gough, D. O. (1981, November). Solar Interior Structure and Luminosity Variations. *Solar Physics*, *74*, 21–34. Retrieved 2022-04-14, from https://ui.adsabs.harvard.edu/abs/1981SoPh...74...21G (ADS Bibcode: 1981SoPh...74...21G) doi: 10.1007/BF00151270

Heymsfield, A. J., Krämer, M., Luebke, A., Brown, P., Cziczo, D. J., Franklin, C., ... Tricht, K. V. (2017, January). Cirrus Clouds. *Meteorological Monographs*, *58*(1), 2.1–2.26. Retrieved 2022-02-21, from https://journals.ametsoc.org/view/journals/amsm/58/1/amsmonographs-d-16-0010.1.xml (Publisher: American Meteorological Society Section: Meteorological Monographs) doi: 10.1175/AMSMONOGRAPHS-D-16-0010.1

Ito, Y., Hashimoto, G. L., Takahashi, Y. O., Ishiwatari, M., & Kuramoto, K. (2020, April). H2O2-induced Greenhouse Warming on Oxidized Early Mars. *The Astrophysical Journal*, *893*, 168. Retrieved 2021-07-27, from https://ui.adsabs.harvard.edu/abs/2020ApJ...893..168I doi: 10.3847/1538-4357/ab7db4

Kite, E. S., Steele, L. J., Mischna, M. A., & Richardson, M. I. (2021, May). Warm early Mars surface enabled by high-altitude water ice clouds. *Proceedings of the National Academy of Science*, *118*, 2101959118. Retrieved 2022-04-14, from https://ui.adsabs.harvard.edu/abs/2021PNAS..11801959K (ADS Bibcode: 2021PNAS..11801959K) doi: 10.1073/pnas.2101959118

Krämer, M., Rolf, C., Spelten, N., Afchine, A., Fahey, D., Jensen, E., ... Sourdeval, O. (2020, November). A microphysics guide to cirrus - Part 2: Climatologies of clouds and humidity from observations. *Atmospheric Chemistry & Physics*, *20*, 12569–12608. Retrieved 2022-02-21, from https://ui.adsabs.harvard.edu/abs/2020ACP....2012569K (ADS Bibcode: 2020ACP....2012569K) doi: 10.5194/acp-20-12569-2020

Krämer, M., Schiller, C., Afchine, A., Bauer, R., Gensch, I., Mangold, A., ... Spichtinger, P. (2009, June). Ice supersaturations and cirrus cloud crystal numbers. *Atmospheric Chemistry & Physics*, *9*, 3505–3522. Retrieved 2021-08-04, from https://ui.adsabs.harvard.edu/abs/2009ACP.....9.3505K doi: 10.5194/acp-9-3505-2009

Lamquin, N., Stubenrauch, C. J., Gierens, K., Burkhardt, U., & Smit, H. (2012, January). A global climatology of upper-tropospheric ice supersaturation occurrence inferred from the Atmospheric Infrared Sounder calibrated by MOZAIC. *Atmospheric Chemistry & Physics*, *12*, 381–405. Retrieved 2021-08-

04, from https://ui.adsabs.harvard.edu/abs/2012ACP....12..381L doi: 10.5194/acp-12-381-2012

Lanza, N. L., Wiens, R. C., Arvidson, R. E., Clark, B. C., Fischer, W. W., Gellert, R., … Zorzano, M.-P. (2016, July). Oxidation of manganese in an ancient aquifer, Kimberley formation, Gale crater, Mars. *Geophysical Research Letters*, *43*, 7398–7407. Retrieved 2021-08-19, from https://ui.adsabs.harvard.edu/abs/2016GeoRL..43.7398L (ADS Bibcode: 2016GeoRL..43.7398L) doi: 10.1002/2016GL069109

Maltagliati, L., Montmessin, F., Fedorova, A., Korablev, O., Forget, F., & Bertaux, J. L. (2011, September). Evidence of Water Vapor in Excess of Saturation in the Atmosphere of Mars. *Science*, *333*, 1868. Retrieved 2021-08-04, from https://ui.adsabs.harvard.edu/abs/2011Sci...333.1868M doi: 10.1126/science.1207957

Manabe, S., & Wetherald, R. T. (1967, May). Thermal Equilibrium of the Atmosphere with a Given Distribution of Relative Humidity. *Journal of Atmospheric Sciences*, *24*, 241–259. Retrieved 2022-04-14, from https://ui.adsabs.harvard.edu/abs/1967JAtS...24..241M (ADS Bibcode: 1967JAtS...24..241M) doi: 10.1175/1520-0469(1967)024⟨0241:TEOTAW⟩2.0.CO;2

Murray, B. J., & Jensen, E. J. (2010, January). Homogeneous nucleation of amorphous solid water particles in the upper mesosphere. *Journal of Atmospheric and Solar-Terrestrial Physics*, *72*, 51–61. Retrieved 2022-02-21, from https://ui.adsabs.harvard.edu/abs/2010JASTP..72...51M (ADS Bibcode: 2010JASTP..72...51M) doi: 10.1016/j.jastp.2009.10.007

Poncin, L., Kleinböhl, A., Kass, D. M., Clancy, R. T., Aoki, S., & Vandaele, A. C. (2022, March). Water vapor saturation and ice cloud occurrence in the atmosphere of Mars. *Planetary and Space Science, Volume 212, article id. 105390.*, *212*, 105390. Retrieved 2022-02-21, from https://ui.adsabs.harvard.edu/abs/2022P%26SS..21205390P/abstract doi: 10.1016/j.pss.2021.105390

Ramirez, R. M., & Kasting, J. F. (2017, January). Could cirrus clouds have warmed early Mars? *Icarus*, *281*, 248–261. Retrieved 2021-08-06, from https://ui.adsabs.harvard.edu/abs/2017Icar..281..248R doi: 10.1016/j.icarus.2016.08.016

Ramirez, R. M., Kopparapu, R., Zugger, M. E., Robinson, T. D., Freedman, R., & Kasting, J. F. (2014, January). Warming early Mars with CO2 and H2. *Nature Geoscience*, *7*, 59–63. Retrieved 2022-02-21, from https://ui.adsabs.harvard.edu/abs/2014NatGe...7...59R (ADS Bibcode: 2014NatGe...7...59R) doi: 10.1038/ngeo2000

Sagan, C., & Mullen, G. (1972, July). Earth and Mars: Evolution of Atmospheres and Surface Temperatures. *Science*, *177*, 52–56. Retrieved 2022-04-14, from https://ui.adsabs.harvard.edu/abs/1972Sci...177...52S (ADS Bibcode: 1972Sci...177...52S) doi: 10.1126/science.177.4043.52

Segura, T. L., McKay, C. P., & Toon, O. B. (2012, July). An impact-induced, stable, runaway climate on Mars. *Icarus*, *220*, 144–148. Retrieved 2022-04-14, from https://ui.adsabs.harvard.edu/abs/2012Icar..220..144S (ADS Bibcode: 2012Icar..220..144S) doi: 10.1016/j.icarus.2012.04.013

Segura, T. L., Toon, O. B., & Colaprete, A. (2008, November). Modeling the environmental effects of moderate-sized impacts on Mars. *Journal of Geophysical Research (Planets)*, *113*, E11007. Retrieved 2022-04-14, from https://ui.adsabs.harvard.edu/abs/2008JGRE..11311007S (ADS Bibcode: 2008JGRE..11311007S) doi: 10.1029/2008JE003147

Segura, T. L., Toon, O. B., Colaprete, A., & Zahnle, K. (2002, December). Environmental Effects of Large Impacts on Mars. *Science*, *298*, 1977–1980. Retrieved 2022-04-14, from https://ui.adsabs.harvard.edu/abs/2002Sci...298.1977S (ADS Bibcode: 2002Sci...298.1977S) doi:

10.1126/science.1073586
Turbet, M., & Forget, F. (2019, April). The paradoxes of the Late Hesperian Mars ocean. *Scientific Reports*, *9*, 5717. Retrieved 2021-12-09, from https://ui.adsabs.harvard.edu/abs/2019NatSR...9.5717T (ADS Bibcode: 2019NatSR...9.5717T) doi: 10.1038/s41598-019-42030-2
Turbet, M., & Forget, F. (2022, March). *3-D Global modelling of the early martian climate under a dense CO2+H2 atmosphere and for a wide range of surface water inventories* (Tech. Rep.). Retrieved 2022-02-21, from https://ui.adsabs.harvard.edu/abs/2021arXiv210310301T (Publication Title: arXiv e-prints ADS Bibcode: 2021arXiv210310301T Type: article)
Turbet, M., Forget, F., Head, J. W., & Wordsworth, R. (2017, May). 3D modelling of the climatic impact of outflow channel formation events on early Mars. *Icarus*, *288*, 10–36. Retrieved 2021-12-09, from https://ui.adsabs.harvard.edu/abs/2017Icar..288...10T (ADS Bibcode: 2017Icar..288...10T) doi: 10.1016/j.icarus.2017.01.024
Urata, R. A., & Toon, O. B. (2013, September). Simulations of the martian hydrologic cycle with a general circulation model: Implications for the ancient martian climate. *Icarus*, *226*, 229–250. Retrieved 2022-04-14, from https://ui.adsabs.harvard.edu/abs/2013Icar..226..229U (ADS Bibcode: 2013Icar..226..229U) doi: 10.1016/j.icarus.2013.05.014
Vali, G., DeMott, P. J., Möhler, O., & Whale, T. F. (2015, September). Technical Note: A proposal for ice nucleation terminology. *Atmospheric Chemistry & Physics*, *15*, 10263–10270. Retrieved 2022-02-21, from https://ui.adsabs.harvard.edu/abs/2015ACP....1510263V (ADS Bibcode: 2015ACP....1510263V) doi: 10.5194/acp-15-10263-2015
Wordsworth, R., Forget, F., Millour, E., Head, J. W., Madeleine, J. B., & Charnay, B. (2013, January). Global modelling of the early martian climate under a denser CO2 atmosphere: Water cycle and ice evolution. *Icarus*, *222*, 1–19. Retrieved 2021-08-13, from https://ui.adsabs.harvard.edu/abs/2013Icar..222....1W (ADS Bibcode: 2013Icar..222....1W) doi: 10.1016/j.icarus.2012.09.036
Wordsworth, R. D. (2016, June). The Climate of Early Mars. *Annual Review of Earth and Planetary Sciences*, *44*, 381–408. Retrieved 2021-07-27, from https://ui.adsabs.harvard.edu/abs/2016AREPS..44..381W doi: 10.1146/annurev-earth-060115-012355